Journal of Theoretical Biology 269 (2011) 307–317

Contents lists available at ScienceDirect

Journal of Theoretical Biology

journal homepage: www.elsevier.com/locate/yjtbi

Effects of snout dimensions on the hydrodynamics of suction feeding in juvenile and adult seahorses

Gert Roos [a,*], Sam Van Wassenbergh [a], Peter Aerts [a,b], Anthony Herrel [a,c], Dominique Adriaens [d]

[a] Department of Biology, Universiteit Antwerpen, Universiteitsplein 1, B-2610 Antwerpen, Belgium
[b] Department of Movement and Sports Sciences, Ghent University, Watersportlaan 2, B-9000 Gent, Belgium
[c] Département d'Ecologie et de Gestion de la Biodiversité, Muséum National d'Histoire Naturelle, 57 rue Cuvier, Case postale 55,75231, Paris Cedex 5, France
[d] Evolutionary Morphology of Vertebrates, Ghent University, K.L. Ledeganckstraat 35, B-9000 Gent, Belgium

ARTICLE INFO

Article history:
Received 19 May 2010
Received in revised form
18 October 2010
Accepted 20 October 2010
Available online 26 October 2010

Keywords:
Syngnathidae
Feeding
Expansion
Ontogeny
CFD

SUMMARY

Seahorses give birth to juveniles having a fully functional feeding apparatus, and juvenile feeding behaviour shows striking similarities to that of adults. However, a significant allometric growth of the snout is observed during which the snout shape changes from relatively short and broad in juveniles to relatively long and slender in adults. Since the shape of the buccal cavity is a critical determinant of the suction performance, this snout allometry will inevitably affect the suction feeding ability. To test whether the snout is optimised for suction feeding throughout an ontogeny, we simulated the expansion of different snout shapes varying from extremely long and slender to short and broad for juvenile and adult snout sizes, using computational fluid dynamic models. Our results showed that the snout diameter at the start of the simulations is involved in a trade-off between the realizable suction volume and expansion time on the one hand (improving with larger initial diameters), and maximal flow velocity on the other hand (improving with smaller initial diameters). Moreover suction performance (suction volume as well as maximal attainable flow velocity) increased with decreasing snout length. However, an increase in snout length decreases the time to reach the prey by the cranial rotation, which may explain the prevalence of long snouts among syngnathid fishes despite the reduced suction performance. Thus, the design of the seahorse snout revolves around a trade-off between the ability to generate high-volume suction versus minimisation of the time needed to reach the prey by the cranial rotation.

1. Introduction

Juveniles often show strong morphological differences in comparison to adults. During ontogeny, these differences may be reflected in positive or negative allometric growth in certain morphological features (Reilly, 1995; Richard and Wainwright, 1995; Carrier, 1996; Meyers et al., 2002; Vincent et al., 2004) or in the development of novel morphological structures or linkages at a certain age (Adriaens et al., 2001; Hunt von Herbing, 2001; Larson, 2005). These differences in morphology in turn often result in differences in performance or behaviour during ontogeny as shown by a number of previous studies (Schmidt-Nielsen, 1984; Herrel and Gibb, 2006).

During early ontogeny, vertebrates often show a reduced feeding performance compared to their adult life stages (Herrel and Gibb, 2006). For an instance, bite force shows a positive allometry with respect to body and head dimensions in fish (Hernandez and Motta, 1997), lizards (Meyers et al., 2002), turtles (Herrel and O'Reilly, 2006), crocodiles (Erickson et al., 2003), birds (Herrel et al., 2005) and mammals (Binder and Van Valkenburgh, 2000). Similar to the bite force, the linear velocity of upper and lower jaw tips also increases with increasing body size, suggesting that larger animals are able to capture larger and more elusive prey (Richard and Wainwright, 1995; Meyers et al., 2002; Herrel and Gibb, 2006; Hernandez, 2000). Previous studies also suggested that the suction feeding performance, the most common prey capture strategy of aquatic vertebrates, increases with increasing body size (Robinson and Motta, 2002; Van Wassenbergh et al., 2006; Holzman et al., 2008a, 2008b), which may explain why larger animals show a more diverse diet than smaller conspecifics.

Whereas most suction feeders require a period of maturation involving a gradual improvement in their feeding performance after hatching, seahorses give birth to young with a fully functional feeding system specialized for the pivot feeding, a special type of suction feeding (Van Wassenbergh et al., 2009a, 2009b; Leysen et al., 2010). Exceptionally high rotational velocities of the snout toward the prey (first phase of the pivot feeding), followed by relatively large buccal expansions (second phase of the pivot feeding) were observed in juvenile *Hippocampus reidi* compared

* Correspondence to: Departemente d'Biologie, Universiteit Antwerpen, Laboratory for Functional Morphology, Universiteitsplein 1, Belgium.
Tel.: +32 3820 22 60; fax: +32 3820 22 71.
E-mail address: Gert.Roos@ua.ac.be (G. Roos).

0022-5193/$ - see front matter © 2010 Elsevier Ltd. All rights reserved.
doi:10.1016/j.jtbi.2010.10.023

to adults (Roos et al., 2010). The high performance of newborn seahorses can be explained by the fact that male seahorses provide post-zygotic care for the embryos inside the brood pouch, allowing the juveniles to be born at a later developmental stage involving a greater degree of maturation of the feeding system (Van Wassenbergh et al., 2009a, 2009b; Kornienko, 2001). Despite similar prey capture behaviour, and at first sight a high performance in both newborn and adult seahorses, considerable allometric growth of head and snout dimensions occurs during ontogeny in seahorses (Roos et al., 2010; Choo and Liew, 2006). Newborn juveniles bear a relative short and broad snout, which becomes significantly longer and more slender as they grow. A recent study showed that both juveniles and adults show a snout length that is approximately optimal to reach the prey as fast as possible by rotating the head for a given width of the snout (Roos et al., 2010). Therefore, the allometry in the snout length could be a functional response to the differences in snout width between juveniles and adults. However, since the study by Roos et al. (2010) only focused on the optimisation of the snout length (and not width or height) for performance during the first phase of pivot feeding (i.e. head rotation), this means that it remains currently unknown whether the observed allometry in snout dimensions in seahorses is driven by functional demands.

Indeed, the allometric increase of head and snout dimensions may have important consequences for the second phase of the pivot feeding: the generation of suction by buccal expansion. During the buccal expansion, a negative pressure is generated inside the buccal cavity, which causes the water in front of the predator to flow towards and into the predator's mouth (Lauder, 1985). When the suction force overcomes the prey's inertia and escape response, the prey with the surrounding water are drawn into the suction feeder's mouth (Van Wassenbergh et al., 2006; Wainwright and Day, 2007). A study by Van Wassenbergh et al. (2006) showed that the shape of the buccal cavity at rest has a very important effect on the suction performance. Since the absolute size of the buccal cavity strongly also influences the flow patterns and energetics of the buccal expansion (Drost et al., 1988), the shape change in the buccal cavity during ontogeny of *Hippocampus reidi* may be a response to the hydrodynamics of the suction feeding.

This paper aims to address the question whether the snout allometry in seahorses can be explained as a response to hydrodynamic constraints. In this context, two alternative scenarios could explain the snout allometry in *H. reidi*: (1) the juveniles expelled from the male's brood pouch have a snout that is suboptimal for suction feeding, due to developmental or other constraints. Therefore, the snout proportions change rapidly to bypass the suboptimal stage as quickly as possible. (2) The snout dimensions in newborn juveniles are already optimised for the suction feeding. The snout allometry is dictated by the changing hydrodynamic constraints during growth (for example, the gradually less viscous flow regime). We will test these hypotheses by hydrodynamic modelling of the snout expansion in juvenile and adult *Hippocampus reidi*.

2. Material and methods

2.1. Mesh construction

In analogy with Van Wassenbergh and Aerts, 2009, a 2D axisymmetric, unstructured triangular mesh was created using GAMBIT 2.3.16 (Ansys, Lebanon, NH, USA). In this mesh, the snout was modelled as a cylinder (open at the mouth side and closed at the opercular side) (Fig. 1A, B). A cone was attached to this cylinder to avoid abrupt changes in the flow pattern (Fig. 1B). A cylindrical open boundary surface enclosed the flow domain. The distances of the nodes were smaller near the snout (0.006 and 0.10 mm, for

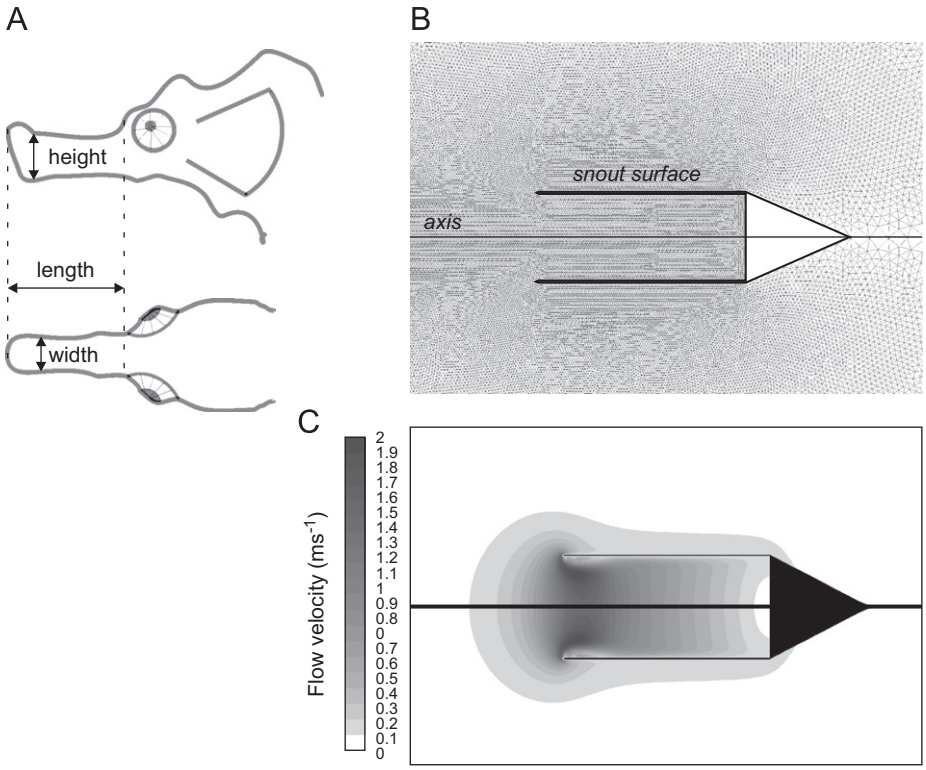

Fig. 1. Illustration of the 2D axisymmetric, triangular mesh used in the simulations (A). Snout height, width and length were used as an input to set the initial dimensions of the cylindrical snout model. This mesh was imported into FLUENT in which radial abduction of the snout was simulated (C). Note that the average measured adult snout was used in the representative figures. Similar methods were used to model juvenile snout expansion.

juveniles and adults, respectively) than those at the boundary of the domain (0.08 and 1 mm, for juveniles and adults, respectively) to increase the accuracy of the results of the simulations.

Previous studies used more complex cylinder or cone geometries to calculate flow velocities and pressures inside the buccal cavity, using hydrodynamically simplified analytical models (Van Wassenbergh et al., 2006; Drost et al., 1988; Roos et al., 2009; Muller et al., 1982). They argued that a single expanding cylinder should better be divided into a series of smaller cylinders or cones, which expand at different timings to mimic the typical anterior to posterior expansion sequence of the buccal cavity more accurately. Since the expansion of the snout in the seahorse *Hippocampus reidi* resembles a radially expanding cylinder, and the prey is always engulfed long before the more posterior elements (e.g. opercula) start to expand (Roos et al., 2009), we chose this simple, cylindrical expansion as a model system.

The lateral and dorsal sides of the head of 20 juveniles (1–3 days old) and 10 adults preserved in neutralised and buffered formalin solution were photographed digitally. The snout length, height and width of each individual were measured in each photograph using the ImageJ software (1.41 m, W. Rasband, National Institute of Mental Health, Bethesda, MA, USA). The distance between the snout tip and the anterior part of the frontal bone (anterior to the eye) was defined as the snout length (Fig. 1A). Snout height was measured as the distance between the articulation of the lower jaw with the quadrate and the anterior tip of the vomer (Fig. 1A). The distance between the left and right articulations of the lower jaw with the quadrate was defined as the snout width (Fig. 1A). The mean snout length was taken for the juvenile and adult age class to represent the length of the model. To create an axially symmetric model, the square root of the product of the average snout width and the average snout height was taken to obtain the radius of the model (Fig. 1B). In this way, cross-sectional areas and volume remain unaffected (Van Wassenbergh and Aerts, 2009).

2.2. Mesh motion

The computational fluid dynamics (CFD) simulation of the expansion of the model was performed in FLUENT 6.3.16 (Ansys, Lebanon, NH, USA). To simulate the axial abduction of the snout, FLUENT-user-defined functions (DEFINE-CG-MOTION UDFs) were utilised. The maximal expansion and the expansion time of the juvenile and adult model were based on data derived from previous studies (Van Wassenbergh et al., 2009a, 2009b; Roos et al., 2009). All UDFs were compiled using Microsoft Visual Studio 2005. Radial movement of the entire snout was simulated using a sine function, in which the expansion velocity increases to a maximum halfway the expansion (Fig. 1C). Because expansion is the same at each point along the axis of the cylinder, the initial diameter of the cylinder at the open side is also the initial mouth diameter. Note that, there is no forward movement of the model during the simulations, which is also found in seahorse feeding (Roos et al., 2010).

Numerical algorithms were used to update the mesh relative to the input motion in each time step using two methods. The first method was a spring-based smoothing method. Here, the edges connecting the nodes were considered as springs with a spring factor of 1.0 and a boundary node relaxation factor of 1.0, and a convergence tolerance of 0.001 (Van Wassenbergh and Aerts, 2009). In the second method, cells which became critically small ($<1\times10^{-6}$ and $<5\times10^{-6}$ mm for the juvenile and adult models, respectively) or large ($>5\times10^{-5}$ and $>5\times10^{-5}$ mm) or too skewed (>0.6, with skewness defined as the difference in triangle shape between an equilateral triangle and a triangle with an equivalent volume) during mesh motion were remeshed by FLUENT.

2.3. CFD settings

In FLUENT 6.3.16, unsteady flow simulations were performed, in which laminar flow was assumed (Van Wassenbergh and Aerts, 2009). The no-slip wall condition was enforced at the moving surfaces of the snout, which is the default condition for models of viscous flow in FLUENT 6.3. The cylindrical open boundary surface of the domain (Fig. 1C) was modelled as a pressure-outlet, where a gauge pressure of zero applies (i.e. no changes in pressure due to the assumption of fish at this boundary) and a backflow normal to the boundary.

The pressure-based solver (chosen to obtain fast-converging solutions) was used with a node-based Green-Gauss gradient treatment. The latter achieves higher accuracy in unstructured triangular grids compared to the cell-based gradient treatment. The first-order implicit unsteady formulation option was used in the simulation, because moving mesh simulations currently only work with first-order time advancement. The standard pressure discretization scheme was used for the pressure calculation and a second-order upwind scheme was used for momentum equations. The pressure–velocity coupling was solved using the SIMPLE scheme. The latter is a discretization method that uses a relationship between velocity and pressure corrections to enforce mass conservation and to obtain the pressure field. A constant amount of 125 time steps were used, consequently the time step size was 0.00004 and 0.00016 s for the juvenile and adult simulations, respectively. A maximum of 50 iterations per time step was sufficient to reach convergence.

2.4. Calculation of power requirement

The total power required from the feeding system to realize the buccal expansion that was prescribed was calculated by taking the product of the radial component of the pressure forces and radial velocities of each of the two faces (i.e. external and internal mesh surface subdivisions) of the modelled buccal cavity, and by summing these powers for the entire buccal surface. This calculation was automatically performed after each time step by including a DEFINE_EXECUTE_AT_END user-defined function in the program (Van Wassenbergh and Aerts, 2009).

Recent studies showed that the work input of the epaxial and hypaxial musculature provides the largest fraction of total suction power in fish (Carroll et al., 2004; Carroll and Wainwright, 2006; Coughlin and Carroll, 2006; Van Wassenbergh et al., 2008). In pivot feeders, the kinetic energy delivered by the epaxial muscles is primarily driven by an elastic recoil of the epaxial muscles and tendons (Van Wassenbergh et al., 2008; Muller, 1987). When maximal head rotation is reached, the kinetic energy is either dampened by cranial structures or (partially) transferred and used to expand the snout. For the purpose of the simulations, we assume that the energy needed to expand the buccal cavity has the same order of magnitude as the kinetic energy needed to rotate the head.

The maximum calculated work input (integral of instantaneous power over time) of each age class was compared to the power requirement to rotate the head in each age class to evaluate whether the magnitude of the calculated power requirement was realistic. First, the kinetic energy of the head rotation was calculated as the product of the head's moment of inertia and the head's angular velocity squared divided by two (Roos et al., 2010). This kinetic energy was multiplied by 1.5 to account for the added mass (Roos et al., 2010; Van Wassenbergh et al., 2008). Next, we assumed that the hypaxial muscles can provide an additional 10%

to the kinetic energy of the epaxial muscles, since the mass of the hypaxial muscles is ten times less than that of the epaxial muscles (G. Roos, unpublished data).

2.5. Simulation of different snout shapes

The average measured snout radius and snout length of the juveniles and adults were multiplied by 0.5, 0.75, 1, 1.5 and 2 to obtain 25 different snout morphologies for each age class ranging from long and slender snouts to short and broader snouts. Two sets of simulations were performed for each juvenile and adult snout morphology. In the first set of simulations, we assumed that potential changes in the muscle–tendon physiology and the gearing properties of force and velocity within the buccal expansion system are highly constrained, so that suction power can only be generated within a fixed time interval. In these simulations, the expansion volume was adjusted to meet our general assumption that the amount of work input from the musculature remains equal. In the second set of simulations, we assumed that changes to the morphology of the cranial elements of the expansion system are highly constrained, so that only a fixed, maximal expansion volume can be realized. In these simulations, the expansion duration was varied to meet our general assumption that the amount of work input from the musculature remains equal. Consequently, depending on which type of morphological, behavioural or physiological changes are most likely to occur by means of evolution or via phenotypical plasticity, one would either expect the first set of simulations (in case of a variable cranial expansion magnitude) or the second set of simulations (in case of a variable duration of the suction power generation) to be more relevant. Note, however, that probably a combination of both types of modifications would occur in nature, but we must separate these two effects (expansion duration and expansion magnitude) for our model to become determined.

As mentioned above, in the first set of simulations, we assumed that the expansion time remains constant. Per snout morphology, we ran up to five simulations with different maximum snout expansions, which resulted in different work inputs. Linear interpolations were performed to obtain the maximal volume change that a particular snout morphology can generate with a constant amount of expansion time and work. In the second set of simulations, we assumed that the volume change realised by expansion remains constant (equal amount of water sucked into the snout). Again, up to five simulations were run to obtain a set of different expansion times with different work inputs. Interpolations enabled us to pinpoint the minimal expansion time needed to expand up to a constant volume change the given, realistic estimate of constant work input. In turn, this result was used to obtain the maximal flow velocity at the gape and the minimal pressure inside the buccal cavity.

In addition, the growth trajectory of the snout shape ranging from early juvenile to adult was superimposed on the adult hydrodynamic simulation results to investigate the implications of ontogenetic snout shape changes on the characteristics of suction. This trajectory is based on measurements of the snout dimensions (length, height and width) of seahorse specimens of different ages ranging from 1 day old to 20 weeks old (adult). To eliminate absolute size differences, the snout dimensions in this ontogenetic series were scaled up to the buccal volume of the adult snout.

3. Results

3.1. Hydrodynamic effects of differences in length and initial diameter for a given expansion time and work input

In the following simulations, the radial expansion magnitude was adjusted for each cylindrical CFD model with a different starting geometry (i.e. length and initial diameter) such that the expansion always required the same work input (0.6×10^{-9} and 6×10^{-3} J for juveniles and adults, respectively) from the animal's feeding musculature. The time needed to perform the expansion (5 ms for juveniles and 20 ms for adults) was not adjusted.

3.1.1. Juveniles

Our CFD simulations showed that the suction generated by radial expansion of a cylinder that is relatively broader and shorter than the cylinder modelled based on the dimensions of the snout of a juvenile seahorse allowed a larger volume increase for a given work input (Fig. 2A). For instance, the average measured juvenile snout has a length of 0.7 mm and an initial diameter of 0.32 mm and expanded by 0.08 mm^3 during suction feeding. A relatively broader and shorter snout with a length of 0.35 mm and an initial diameter of 0.64 mm can be expanded by 0.2 mm^3 for the same work input, which is approximately three times higher (Fig. 2A). In contrast, a relatively long and slender cylinder with a length of 1.4 mm and an initial diameter of 0.16 mm could only expand by 0.01 mm^3, which is eight times less compared to the original model of the juvenile seahorse (Fig. 2A).

The maximal flow velocity calculated at the gape increased when the starting geometry of the cylinder was made shorter and more slender (Fig. 2C). The maximal flow velocity of the expanding cylinder modelled after the juvenile snout was 0.2 ms^{-1}. Starting the expansion from a more slender and shorter cylinder (length = 0.35 mm, initial diameter = 0.16 mm), increased the maximal flow velocity by 2 times to 0.3 ms^{-1} (Fig. 2C). In contrast, a relatively longer and broader snout (length = 1.4 mm and initial diameter = 0.64 mm) generated a maximal flow velocity of 0.07 ms^{-1}, which is 3 times less than the peak velocity output for the original model (Fig. 2C).

The maximal sub-ambient pressure difference at the expanding cylinder surface increases predominantly as a function of decreasing initial diameter (Fig. 2E). For the model of the average juvenile snout, the maximal sub-ambient pressure difference was 69 Pa. This pressure difference is 2 times higher compared to the sub-ambient pressure difference of 41 Pa induced by an expanding cylinder with the same length (0.70 mm), but with an initial diameter of 0.64 mm (Fig. 2E). If the cylinders length was kept at 0.7 mm and the initial diameter reduced to 0.16 mm, a sub-ambient pressure difference of 228 Pa was generated during suction, which is 3 times higher than the value calculated for the original juvenile seahorse model (Fig. 2E).

3.1.2. Adults

For models of adult seahorse snouts, the maximum attainable volume for a given expansion time and work input from the musculature increases with a relatively shorter and broader initial geometry (Fig. 2B). The model of the average adult snout (length = 11 mm, initial diameter = 2.28 mm) was able to increase by 157 mm^3 during suction, which is 4 times higher than the 41 mm^3 expansion achieved by a snout with a length of 22 mm and a diameter of 1.14 mm (Fig. 2B). On the other hand, a snout with a length of 5.5 mm and an initial diameter of 4.56 mm could expand by 427 mm^3 for the same work input, which is 3 times higher than our original adult *Hippocampus reidi* model (Fig. 2B).

The maximum flow velocity increases mainly with decreasing initial snout diameter (Fig. 2D). The highest flow velocity of 1.6 ms^{-1} is found for a cylinder with a length of 11 mm and an initial diameter 1.14 mm, which is slightly higher than the maximal flow velocity of 1.2 ms^{-1} generated by the model of the average adult snout (length = 11 mm, initial diameter = 2.28 mm) (Fig. 2D). When this 11 mm long cylinder becomes broader (initial diameter = 4.56 mm), the maximal flow velocity decreases to 0.9 ms^{-1}, which is 2 times lower than the flow velocity attained by the original adult *Hippocampus reidi* snout model (Fig. 2D).

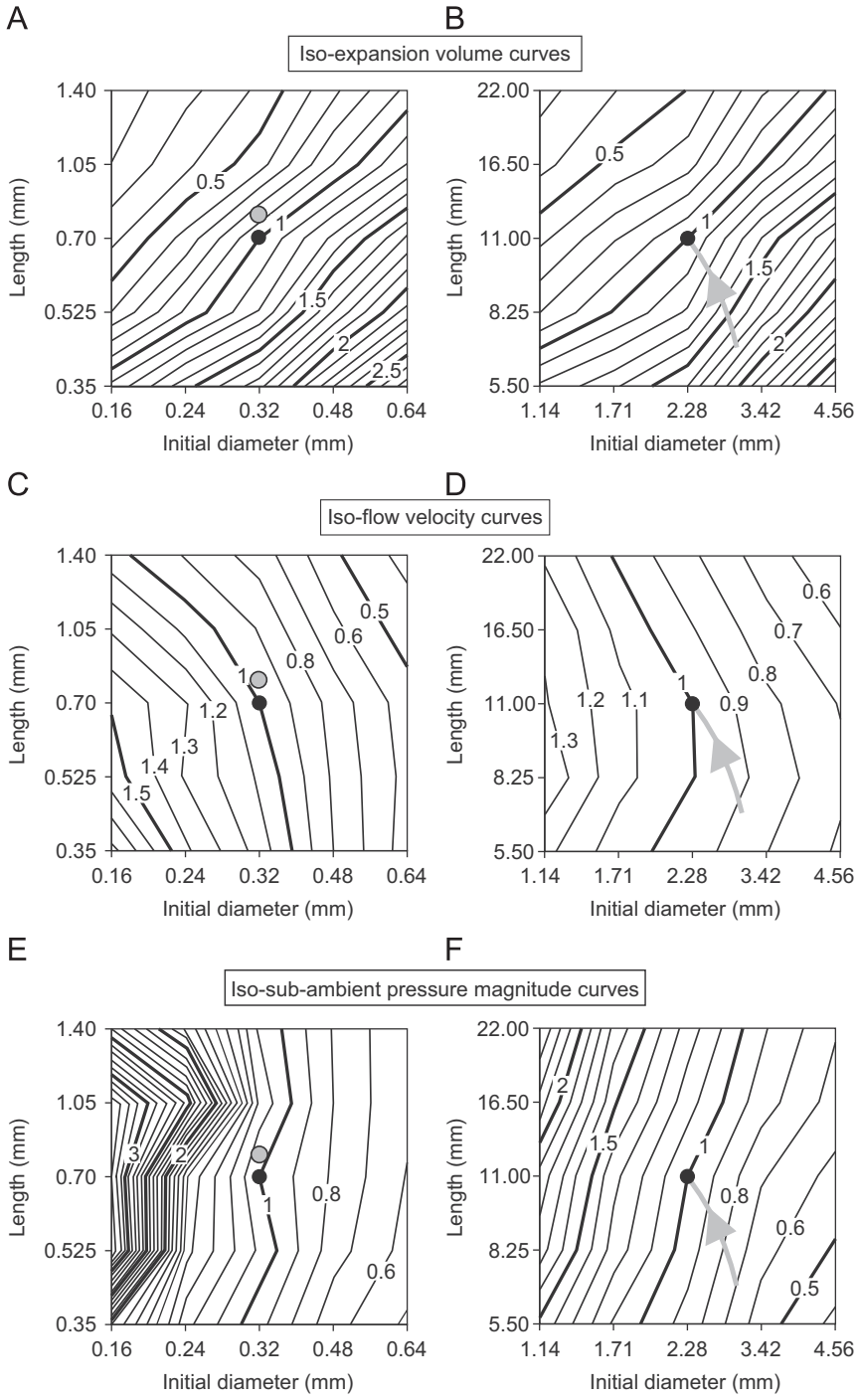

Fig. 2. The results of the CFD simulations in which the work input and the expansion time were unchanged for different snout shapes. The values of realised volume expansion (A, B), flow velocity at the mouth aperture (C, D) and sub-ambient pressure magnitude (E, F) are shown as proportions relative to the model output of the average measured snout shape (black circle) for juveniles (A, C, E) and adults (B, D, F). In the juvenile column, the snout length optimised for head rotation (based on data of Roos and colleagues (Roos et al., 2010)) predicted by the model of de Lussanet and Muller (2007) was marked as a grey point (for details see text). In the adult column, the grey line represents the growth line of the snout shape from a juvenile of less than one week old to the adult snout shape (snout shape was isometrically scaled to the adult buccal volume).

The maximal sub-ambient pressure difference at the expanding cylinder surface increase with increasing snout length and decreasing initial diameter (Fig. 2F). The maximal sub-ambient pressure difference of the model of the adult *Hippocampus reidi* snout is 2.1 kPa, which is 3 times higher than the maximal sub-ambient pressure difference of 0.8 kPa created by a cylinder with length 5.5 mm and an initial diameter 4.56 mm (Fig. 2F). In contrast, the maximal sub-ambient pressure difference calculated for a cylinder with a length of 22 mm and an initial diameter of 1.14 mm is 4.8 kPa, which is 2 times higher than the value calculated for the original model (Fig. 2F).

3.2. *Hydrodynamic effects of differences in length and initial diameter for a given volume increase and work input*

In the following simulations, the time needed to perform a radial expansion of fixed magnitude (0.08 mm^3 for juveniles and

157 mm^3 for adults) was adjusted for each cylindrical CFD model with a different starting geometry (i.e. length and initial diameter) such that the expansion always required the same work input (0.6×10^{-9} and 6×10^{-3} J for juveniles and adults, respectively) from the animal's feeding musculature.

3.2.1. Juveniles

Suction generated by radial expansion of a relatively longer and more slender cylinder than the one modelled after the snout of a juvenile seahorse caused the expansion time to increase (Fig. 3A). The expansion time for the model of the average measured juvenile *Hippocampus reidi* snout with a length of 0.7 mm and an initial diameter of 0.32 mm was 5 ms. For a long and narrow cylinder (length = 22 mm, initial diameter = 0.16 mm), the shortest realizable expansion increases by 4 times to 19 ms compared to the original juvenile snout model (Fig. 3A). In contrast, for a broader and shorter cylinder (length = 0.35 mm, initial diameter = 0.64 mm), the shortest feasible expansion time decreased to 2 ms,

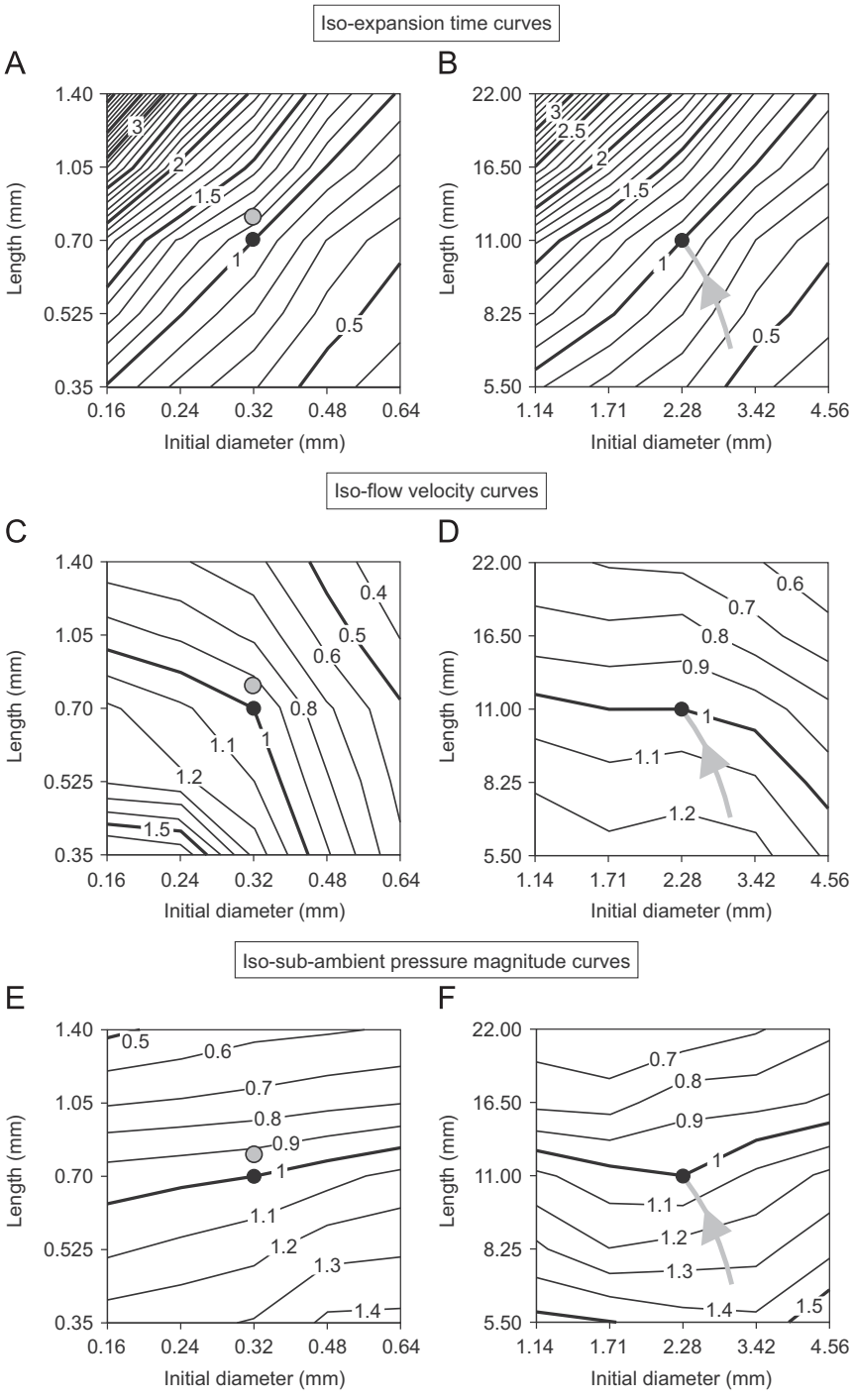

Fig. 3. The results of the CFD simulations in which the work input and the expansion volume were unchanged for different snout shapes. The values of expansion time (A, B), flow velocity at the mouth aperture (C, D) and sub-ambient pressure magnitude (E, F) are shown as proportions relative to the model output of the average measured snout shape (black circle) for juveniles (A, C, E) and adults (B, D, F). In the juvenile column, the snout length optimised for head rotation (based on data from Roos et al. (2010)) predicted by the model of de Lussanet and Muller (2007) was marked as a grey point (for details see text). In the adult column, the grey line represents the ontogenetic line of the snout shape from a juvenile of less than one week old to the adult snout shape (snouts isometrically scaled to match the adult buccal volume).

which is 4 times less compared to the original juvenile seahorse model (Fig. 3A).

The maximum suction-induced flow velocity increases with decreasing cylinder length and initial diameter (Fig. 3C). For example, the maximum flow velocity for the original juvenile snout model (0.2 ms^{-1}) was 1.5 times lower than the maximal velocity of 0.3 ms^{-1} for a relatively narrow and short snout (length=0.35 mm, initial diameter=0.16 mm) (Fig. 3C). When the expanding cylinder's length and initial diameter increased to 1.4 and 0.64 mm, respectively, the maximal velocity decreased to 0.06 ms^{-1}, which is 3 times less than that of the original juvenile seahorse model (Fig. 3C).

The maximum sub-ambient pressure difference appeared to be primarily a function of the length of the expanding cylinder: with increasing cylinder length, the maximum sub-ambient pressure difference decreased (Fig. 3E). The maximum sub-ambient pressure difference of the original juvenile model was 69 Pa. This pressure difference increased to 90 Pa for a snout with an equal initial diameter, but with a snout length of 0.35 mm (Fig. 3E). On the other hand, the maximum sub-ambient pressure difference decreases 2 times to 40 Pa for a snout with an equal initial diameter, but with a length of 1.4 mm (Fig. 3E).

3.2.2. Adults

Similar to the juvenile models, the shortest feasible expansion time in an adult expanding cylinder models increased with increasing cylinder length and decreasing initial diameter (Fig. 3B). The expansion time of the original model of the average measured adult snout was 20 ms, which is 3 times less than the shortest realizable expansion time of 70 ms for a cylinder with length 22 mm and an initial diameter 1.14 mm (Fig. 3B). When the cylinder's starting geometry was made relatively broader and shorter (length=5.5 mm, initial diameter=4.56 mm), the shortest attainable expansion duration decreases 3 times to 7 ms (Fig. 3B).

The maximal flow velocity decreased with increasing cylinder length and initial diameter (Fig. 3D). The maximal flow velocity of the original adult snout model was 1.2 ms^{-1}. The highest maximal flow velocity of 1.5 ms^{-1} in our sample was found for a cylinder with a length of 5.5 mm and an initial diameter 2.28 mm, which is only slightly higher than the original model (Fig. 3D). The lowest maximal flow velocity of 0.7 ms^{-1} was found for the cylinder with a length of 22 mm and an initial diameter 4.56 mm, which is 2 times lower than the original adult snout model (Fig. 3D).

The maximum sub-ambient pressure difference appeared mainly a function of the length of the cylinder, and showed an increase with decreasing snout length (Fig. 3F). The maximum sub-ambient pressure difference for the original adult seahorse model (length=11 mm, diameter=2.28 mm) was 2 kPa, this pressure difference is 2 times higher than the 1 kPa found for a cylinder with the same initial diameter and a length 22 mm (Fig. 3F). For a cylinder with the same initial diameter and with a length of 5.50 mm, the maximum sub-ambient pressure difference was 3 kPa, which is 1.5 times higher than that found for the original model (Fig. 3F).

3.2.3. Ontogeny

As juveniles grow, the snout becomes relatively longer and more slender (Roos et al., 2010). When expansion time and amount of work input are considered constant, this shape change of the snout theoretically results in lower maximal expansion volumes (Fig. 2B), but higher maximal flow velocities at the mouth (Fig. 2D). The maximal pressure inside the buccal cavity also increases gradually as the snout becomes more slender (Fig. 2F). If the expansion volume and work input are assumed constant, the expansion time increases as the juvenile grows (Fig. 3B). As a result, the maximal flow velocity at the mouth and the maximal pressure inside the buccal cavity decreases (Fig. 3D, F).

4. Discussion

In this study, we focussed on the question of why snout allometry is observed during an ontogeny in seahorses (Roos et al., 2010). Undoubtedly, initial snout dimensions affect suction feeding performance (Van Wassenbergh et al., 2006). Therefore, we hypothesised that the observed snout allometry may be related to the optimisation of suction feeding performance. To test this hypothesis, expansions of the snout with a morphology as measured in juveniles and adults, as well as variations of these snout shapes were simulated using computational fluid dynamic models (CFD). The results of these simulations show that an initial snout diameter cannot be considered optimised for suction performance in general, because it is confronted with a trade-off situation between different aspects of suction performance (Figs. 2 and 3). A decrease in the initial snout diameter results in an increase in maximal flow velocity at the gape (Figs. 2C, D and 3C, D), but this has the negative effects of (1) decreasing the amount of water drawn into the mouth by suction (Fig. 2A, B) and (2) increasing the duration of a given expansion for a fixed work input (Fig. 3A, B). Consequently, it is clear that morphology of the suction feeding apparatus represents a complex trade-off between the different aspects of suction hydrodynamics investigated in this study.

Suction performance was evaluated based on four hydrodynamic aspects of suction feeding: volume increase, expansion time, flow velocity and intra-oral pressure. First, the ability to generate a larger volume increase is preferable, because more water can be moved in the direction of the predator's mouth. Therefore, the feeding strike can be initiated when the prey is further away from the mouth and larger prey can be captured (Van Wassenbergh et al., 2006; Higham et al., 2006). Secondly, minimising the expansion time can be crucial because the prey then has less time to react and escape the flow generated by the predator. Thirdly, realisation of higher flow velocities positively influences suction performance, because prey dragged along with this flow will be transported quicker towards and through the buccal cavity (Van Wassenbergh et al., 2009a, 2009b; Wainwright and Day, 2007; Holzman et al., 2008a, 2008b). Finally, since, a previous study showed that large intra-oral pressure drops during suction feeding can considerably stress the skull (Markey et al., 2006), lower sub-ambient pressure magnitudes inside the buccal cavity seem favourable. If the seahorse generates higher sub-ambient pressure magnitudes inside the buccal cavity, it must ensure that the morphology of the snout can cope with these large pressure drops, for example by enforcing the structure of the snout. In turn, these suction feeding characteristics might behave differently in environments with low and high Reynolds numbers. Therefore, we simulated an expansion of the different snout shapes at the juvenile scale as well as the adult scale to account for these possible differences.

Seahorses typically capture small crustaceans suspended in the water column in such a short time that the prey has no time to react. In that case, the approximately neutrally buoyant prey are sucked along with the surrounding water, and the water flow velocity in the vicinity of the prey also describes the velocity of the prey. However, in case prey are attached to the substrate or display an escape response, suction performance can better be quantified by the force excerted on these prey (Van Wassenbergh et al., 2009a, 2009b; Wainwright and Day, 2007; Holzman et al., 2008a, 2008b). Recent studies showed that this force is almost entirely caused by the pressure gradient in the water near the position of the prey (Wainwright and Day, 2007). To complete our quantification of suction performance in our simulations, we also added graphs

showing the effect of initial snout dimensions on the pressure gradient (Fig. 4). The latter is calculated in the mouth opening at the time of peak pressure. Note that, in general, a similar trend for pressure gradient is observed compared to the peak flow velocity (Fig. 4 *versus* Figs. 2 and 3C,D).

As mentioned earlier, in all our simulations we assumed that the work input by the feeding muscles limits suction performance. Given the elastic energy storage and release mechanism used to power suction feeding in syngnathid fish (Van Wassenbergh et al., 2008), work input is the most probable limiting factor in this case. A direct consequence of using a constant work input in our simulations is that sucking a larger parcel of water will inevitably go along with a drop in peak suction flow velocity in our simulations. To asses this classical "suction volume *versus* flow velocity trade-off" (Muller et al., 1982; Higham et al., 2006) more quantitatively, additional simulations were performed in which the expansion volume of the measured adult and juvenile snout was altered (0.5, 0.75, 1.5 and 2 times the original expansion volume) and the expansion time was adjusted to equalize the amount of work input. From these simulations, the maximum flow velocity near the mouth was extracted and divided by the original maximum flow velocity (when the ratio of the expansion volume is 1). In adults, the relation between the relative flow velocity (U) and the relative expansion volume (V) was approximately linear and given by the equation $U = -0.41\,V$, while this relation was $U = -0.33\,V$ in juveniles (intercepts ignored). The negative slope confirms this trade-off. As we are forced to treat the effects of variation in expansion volume and expansion time separately when studying the effects of the initial cylinder shape (see below), it is important to realise that the trade-off between suction volume and flow velocity is still inherently present.

4.1. Snout shape and suction feeding

Whereas that the initial diameter of the snout lies at the heart of a trade-off between expansion volume and flow velocity on one hand and between expansion time and flow velocity on the other hand, our results show that such a trade-off does not exist for the snout length. Analysis of the contour plots suggests that shortening of the snout, while equalizing the work input, increases expansion volume (Fig. 2A, B) and maximum flow velocity (Figs. 2C, D and 3C) and decreases expansion time (Fig. 3A, B). Furthermore, the pressure gradient (the difference between maximal pressure at the mouth and the pressure just in front of the mouth) also increases with decreasing snout length (Fig. 4). Each of these aspects is related to an increase in suction performance for expansion of shorter snouts. Only in adults, when the expansion

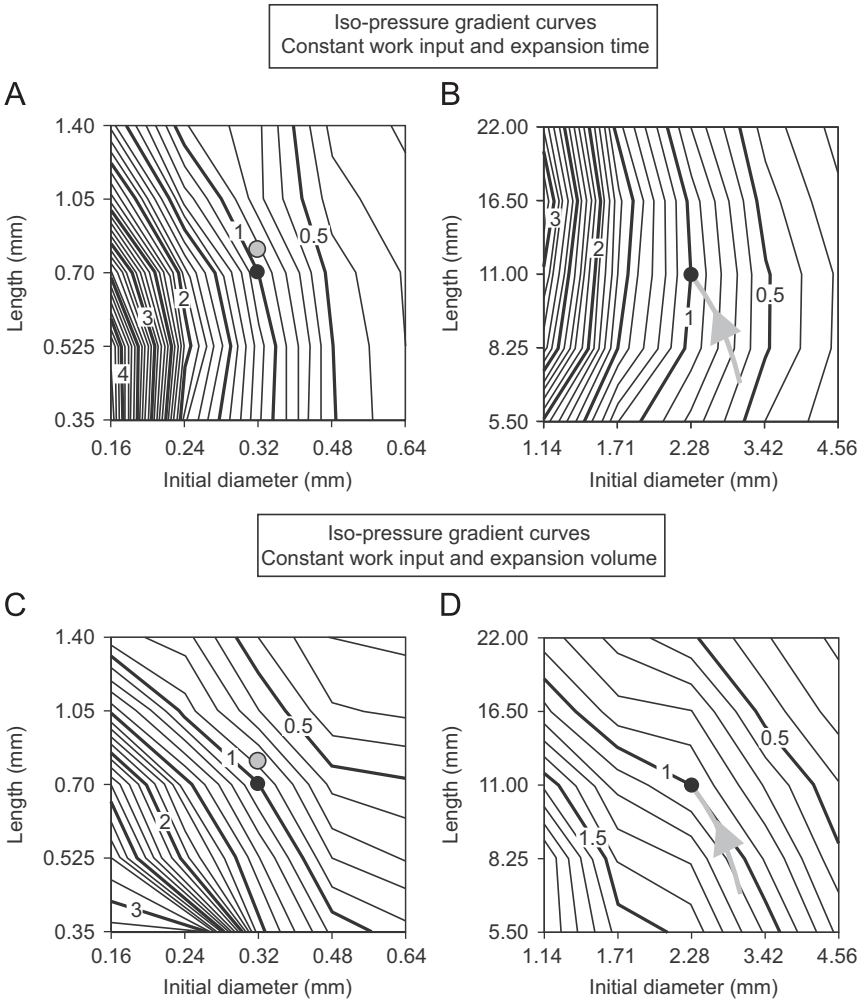

Fig. 4. The results of the pressure gradient for each different juvenile (left column) and adult (right column) snout shape. All values are represented as proportions relative to the model output of the average measured snout (black circle). In the juvenile column, the snout length optimised for head rotation (based on data from Roos et al. (2010)) predicted by the model of de Lussanet and Muller (2007) was marked as a grey point (for details see text). In the adult column, the grey line represents the ontogenetic line of the snout shape from a juvenile of less than one week old to the adult snout shape (snouts isometrically scaled to match the adult buccal volume).

time is allowed to vary in the CFD simulation, flow velocity appears independent of the length of the expanding snout (Fig. 3D).

These findings may explain why long and narrow buccal cavities are not often observed in suction feeding fish. A vast literature on suction feeding in fish exists [e.g. [Van Wassenbergh et al., 2006; Lauder, 1985; Holzman et al., 2008a, 2008b; Liem, 1978; Van Leeuwen and Muller, 1984; Wainwright and Lauder, 1986; Gibb, 1997; Svanbäck et al., 2002; Gibb and Ferry-Graham, 2005]] and most of the fish studied were considered as specialized suction feeding fish. The literature on the buccal shape of suction feeders is limited, however, these studies show that the buccal cavity in rest is relatively wide or deep compared to the buccal cavity length (Van Wassenbergh et al., 2006; Muller et al., 1982; Barel 1983; Van Wassenbergh et al., 2009a, 2009b). This is in contrast with the buccal cavity shape in syngnathids, in which the diameter is relatively small compared to its length (Roos et al., 2009).

There are two possible explanations for the advantages of a long snout related to feeding performance. In the simulations with variable expansion time (Fig. 3), shortening the snout results in higher sub-ambient pressure differences inside the expanding snout (Fig. 3E, F). As we previously argued, it may be preferable for the seahorse to generate suction at the lowest possible intra-oral pressure drops because this ensures minimal stress and strain of the skull (Markey et al., 2006). Note, however, that the effect of snout length on an intra-oral pressure is slightly different in our set of CFD simulation with variable expansion volume. In the latter case, the effect of sub-ambient pressure differences is independent of snout length (Fig. 2E, F). An alternative explanation for the existence of a long snout is related to the distinctive feeding strategy of syngnathids, and will be expanded upon below.

4.2. Snout shape and pivot feeding

Syngnathids have a feeding strategy that is different from that of the other suction feeding fish, and is typically referred to as pivot feeding (Van Wassenbergh et al., 2008; Muller, 1987; de Lussanet and Muller, 2007). During pivot feeding, expansion of the buccal cavity is preceded by cranial rotation (Roos et al., 2009). In most generalised suction feeders, only the cranium is rotated dorsally while the lower jaw rotates ventrally, which causes an additional volume increase during expansion (Lauder, 1985; Gibb and Ferry-Graham, 2005). Syngnathids, on the other hand, rotate the entire head (including upper and lower jaws) to bring the mouth closer to the prey (Roos et al., 2010; Van Wassenbergh et al., 2008; Muller, 1987; de Lussanet and Muller, 2007). Once cranial rotation is near its maximum, the suspensorium starts to abduct (Roos et al., 2009). Consequently, snout shape, in pivot feeders, is not only important to generate suction, but a lower rotational inertia of the snout will decrease the amount of time needed to bring the mouth close to the prey. For instance, a short snout must achieve a larger rotation than a long snout when the prey is located at an identical position relative to the snout (de Lussanet and Muller, 2007). However, since the total moment of inertia of the head increases with an increasing snout length, this negatively affects the angular accelerations during head rotation.

A recent model by de Lussanet and Muller (2007) predicted the optimal snout length in function of a minimisation of the time needed to reach the prey. Interestingly, this model accurately predicts snout lengths of different syngnathid species (de Lussanet and Muller, 2007) as well as the snout length of early juveniles in a seahorse species (Roos et al., 2010). de Lussanet and Muller (2007) use the following formula to calculate reach time:

$$T \approx \frac{d}{l}\sqrt{\frac{J_{total}}{2E}}$$

in which d is the distance between snout tip and prey, l is the distance between snout tip and centre of rotation, E is the amount of kinetic energy provided by the muscles to rotate the head and J_{total} is the total moment of inertia relative to the centre of head rotation. The total moment of inertia is the sum of the total moment of inertia of the snout and that of the head ($J_{total}=J_{head}+J_{snout}$), which are represented by an elliptical cylinder and a half-ellipsoid, respectively (Roos et al., 2010; de Lussanet and Muller, 2007). This formula can be applied to our snout shape variations to calculate the minimal reach time of each snout shape. To do so, we calculated the moment of inertia of each snout shape relative to the centre of head rotation (derived from Roos et al. (2010)) and recalculated l for each snout shape. This means that d, E, J_{head} and the position of the centre of rotation are equal in each snout shape and based on the literature data (Roos et al., 2010).

The shortest minimal reach time is found for a long and slender snout (top left corner, Fig. 5A, B), while the longest minimal reach time is found for a long and broad snout (top right corner, Fig. 5A, B).

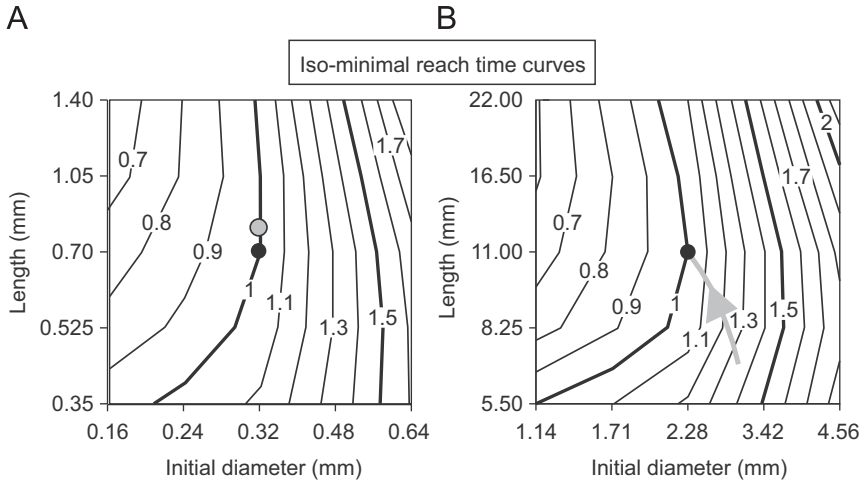

Fig. 5. The results of the minimal reach time (time to reach the prey with the mouth by cranial rotation) for each snout shape obtained by applying the model presented by de Lussanet and Muller (2007). The values are shown as proportions relative to the average measured snout shape (filled circle) for juveniles (left column) and adults (right column). In the juvenile column, the optimal snout length (based on data from Roos et al. (2010)) predicted by the model was marked as a grey point (for details see text). In the adult column, the grey line represents the ontogenetic line of the snout shape from a juvenile of less than one week old to the adult snout shape (snouts isometrically scaled to match the adult buccal volume).

If pivot feeding only includes a fast rotation of the head towards the prey with no subsequent buccal expansion, the long and slender snout would be most suitable. However, as discussed previously, a long snout has the lowest suction performance. Obviously for a long and slender snout, it is of no use to reach the prey extremely fast, if followed by a small volume increase and accompanied by a relatively low flow velocity (see Fig. 2 top left corners of the panels) or followed by a very long expansion time during which no significantly higher flow velocity is generated (see Fig. 3 top left corners of the panels). For example, doubling the length of the snout of our seahorses implies an increase in minimal reach time by at least 10% in juveniles and 20% in adults (Fig. 4A, B), which can be critical for capturing prey.

Apparently, pivot feeders are challenged by an important trade-off between head rotation and snout expansion. Longer and narrower snouts have the highest performance with respect to cranial rotation (performance defined as the ability to minimize prey reach time), but the lowest in some aspects of suction performance. Shorter snouts have a higher suction performance, but the performance of cranial rotation decreases. Perhaps the observed snout shape in animals like *Hippocampus reidi* is simply the best compromise between performance of cranial rotation and suction feeding.

4.3. Ontogeny of snout shape and pivot feeding

Despite that this study suggests that the observed snout shape in *Hippocampus reidi* is a compromise between different aspects of feeding performance for both juveniles as well as adults, it is remarkable that such a pronounced snout allometry exists during ontogeny (Roos et al., 2010; Choo and Liew, 2006). The snout grows from a relatively short and broad snout, as observed in juveniles, to a relatively more slender and long snout. Undoubtedly this snout allometry affects suction feeding and cranial rotation performance. As suggested by a previous study (Roos et al., 2010), the measured snout in early juveniles is slightly shorter than the optimal snout length predicted by the model of de Lussanet and Muller (2007), which means that the minimal time to reach the prey of the measured snout length is higher than that of the calculated optimal snout length (Roos et al., 2010). However, this difference in minimal reach time is less than 1% indicating that the deviation from the optimal solution is relatively small. The consequences for suction feeding of this small deviation of snout length, from the optimum, for cranial rotation, is illustrated by the grey circles in Figs. 2 and 3: our model predicts a slight increase in suction velocity ($<10\%$), an increase in the maximally realizable volume increase ($+15\%$) and a decrease in the time needed to expand the snout (-15%). In adults, on the other hand, the optimal snout length and the measured snout length showed no differences (Roos et al., 2010).

The results of the present study indicate that the trade-off between suction performance and cranial rotation performance is relatively in favour of suction feeding in early juveniles, and becomes more in favour of cranial rotation when the adult snout shape is reached. Scaling of the juvenile snout to the volume of the adult snout (snout volume of juveniles of 1, 2 and 3 weeks are added based on the study by Roos and colleagues (Roos et al., 2010)) shows how the observed snout allometry affects suction feeding and cranial elevation (indicated by the arrow in Figs. 2–5). In the first set of simulations (work input and expansion time are constant, Fig. 2), the existing snout allometry causes a negative effect on expansion volume and maximal pressure, since they both increase, and has a positive effect on the maximal flow velocity. In the second set of simulations (work input and expansion volume are constant, Fig. 3), snout allometry negatively affects expansion time and maximal flow velocity, but positively affects the intra-oral pressure drop which needs to be sustained by the suspensorial bones. In addition, the existing snout allometry has a positive effect on minimal reach time, since the latter decreases during ontogeny (Fig. 5). These findings suggest that snout allometry influences suction performance negatively, but cranial rotation performances positively. In general, newborn juveniles are capable of engulfing relatively larger volumes of water and expanding their snout in less time compared to adults, which indicates a higher suction performance. Kinematic data confirm these model predictions by showing a faster and relatively larger expansion in juvenile *Hippocampus reidi* (Van Wassenbergh et al., 2009a, 2009b). In turn, adults are able to reach their prey faster compared to juveniles, indicating a higher cranial rotation performance. This observed morphology in juveniles optimised towards suction feeding may be the result of their small absolute size favouring a relatively large and fast expansion to maximise the potential prey spectrum. For adults, prey size is likely less of a constraint and faster head rotation velocities may allow them to use more dedicated ambush style foraging tactics, while remaining cryptic for predators.

4.4. Conclusion

This study addressed the question whether the observed snout allometry during an ontogeny in the seahorse *Hippocampus reidi* can be explained by hydrodynamic constraints. To answer this question, we formulated two hypothesises: (1) the juveniles expelled from the male's brood pouch have a snout that is suboptimal for suction feeding. Therefore, the snout proportions change rapidly to bypass the suboptimal stage as quickly as possible. (2) The snout dimensions in newborn juveniles are already optimised for suction feeding and the snout allometry is dictated by the changing hydrodynamic constraints during growth (for example, the gradually less viscous flow regime). Surprisingly, our results indicate that both hypothesises must be rejected since a relatively shorter snout than the snout measured in juveniles is predicted to have a higher suction performance (contra hypothesis 1), while the snout grows in the opposite direction from moving forwards this optimum to become relatively longer in adults (contra hypothesis 2). We argued that the snout length in syngnathids *H. reidi*, in contrast to more typical suction feeders, is constrained by its performance in the quick rotation of the head to bring the mouth close to the prey, which precedes expansion of the snout to generate suction in these fish. Consequently, our study highlights a trade-off between cranial rotation and suction feeding. As the seahorses grow, the observed relative decrease in snout diameter improves the time to reach the prey, but on the other hand this decrease in snout diameter will negatively affect suction performance.

Acknowledgements

G.R. is funded by a Ph.D. grant of the Institute for the Promotion of Innovation through Science and Technology in Flanders (IWT-Vlaanderen). S.V.W. is a postdoctoral fellow of the Fund for Scientific Research, Flanders (FWO-Vl). Supported by FWO-Vl Grant G 053907.

References

Adriaens, D., Aerts, P., Verraes, W., 2001. Ontogenetic shift in mouth opening mechanisms in a catfish (Clariidae, Siluriformes): a response to increasing functional demands. J. Morphol. 247, 197–216.

Binder, W.J., Van Valkenburgh, B.J., 2000. Development of bite strength and feeding behaviour in juvenile spotted hyenas (Crocuta crocuta). J. Zool. (London) 252, 273–283.

Barel, C.D.N., 1983. Towards a constructional morphology of cichlid fishes (Teleostei, Perciformes). Neth. J. Zool. 4, 357–424.
Carrier, D.R., 1996. Ontogenetic limits on locomotor performance. Physiol. Zool. 69, 467–488.
Choo, C.K., Liew, H.C., 2006. Morphological development and allometric growth patterns in the juvenile seahorse *Hippocampus kuda* Bleeker. J. Fish Biol. 69, 426–445.
Carroll, A.M., Wainwright, P.C., Huskey, S.H., Collar, D.C., Turingan, R.G., 2004. Morphology predicts suction feeding performance in centrarchid fishes. J. Exp. Biol. 207, 3873–3881.
Carroll, A.M., Wainwright, P.C., 2006. Muscle function and power output during suction feeding in largemouth bass, *Micropterus salmoides*. Comp. Biochem. Physiol. 143, 389–399.
Coughlin, D.J., Carroll, A.M., 2006. *In vitro* estimates of power output by epaxial muscle during feeding in largemouth bass. Comp. Biochem. Physiol. 145, 533–539.
de Lussanet, M.H.E., Muller, M., 2007. The smaller your mouth, the longer your snout: predicting the snout length of *Syngnathus acus, Centriscus scutatus* and other pipette feeders. J. R. Soc. Interface 4, 561–573.
Drost, M.R., Muller, M., Osse, J.W.M., 1988. A quantitative hydrodynamic model of suction feeding in larval fishes: the role of frictional forces. Proc. R. Soc. B 234, 263–281.
Erickson, G.M., Lappin, A.K., Van Vliet, K.A., 2003. The ontogeny of bite-force performance in American alligator (*Alligator mississipiensis*). J. Zool. (London) 260, 317–327.
Gibb, A.C., 1997. Do flatfish feed like other fishes? A comparative study of percomorph prey capture kinematics. J. Exp. Biol. 200, 2841–2859.
Gibb, A.C., Ferry-Graham, L.A., 2005. Cranial movements during suction feeding in teleost fishes: are they modified to enhance suction production? Zoology 108 141–153.
Hunt von Herbing, I., 2001. Development of feeding structures in larval fish with different life histories: winter flounder and Atlantic cod. J. Fish Biol. 59, 767–782.
Herrel, A., Gibb, A.C., 2006. Ontogeny of performance in vertebrates. Physiol. Biochem. Zool. 79, 1–6.
Hernandez, L.P., Motta, P.J., 1997. Trophic consequences of differential performance: ontogeny of oral jaw crushing performance in the sheepshead, *Archosargus probatocephalus* (Teleostei: Sparidae). J. Zool. (London) 243, 737–756.
Herrel, A., O'Reilly, J.C., 2006. Ontogenetic scaling of bite force in lizards and turtles. Physiol. Biochem. Zool. 79, 31–42.
Herrel, A., Podos, J., Huber, S.K., Hendry, A.P., 2005. Bite performance and morphology in a population of Darwin's finches: implications for the evolution of beak shape. Funct. Ecol. 19, 43–48.
Hernandez, L.P., 2000. Intraspecific scaling of feeding mechanics in an ontogenetic series of zebrafish, *Danio rerio*. J. Exp. Biol. 203, 3033–3043.
Holzman, R., Collar, D.C., Day, S.W., Bishop, K.L., Wainwright, P.C., 2008a. Scaling of suction-induced flows in bluegill: morphological and kinematic predictors for the ontogeny of feeding performance. J. Exp. Biol. 211, 2658–2668.
Higham, T.E., Day, S.W., Wainwright, P.C., 2006. Multidimensional analysis of suction feeding performance in fishes: fluid speed, acceleration, strike accuracy and the ingested volume of water. J. Exp. Biol. 209, 2713–2725.
Holzman, R., Day, S.W., Mehta, R.S., Wainwright, P.C., 2008b. Integrating the determinants of suction feeding performance in centrarchid fishes. J. Exp. Biol. 211, 3296–3305.
Kornienko, E.S., 2001. Reproduction and development in some genera of pipefish and seahorses of the family Syngnathidae. Russ. J. Mar. Biol. 27, S15–S26.
Larson, P.M., 2005. Ontogeny, phylogeny, and morphology in anuran larvae: a morphometric analysis of cranial development and evolution in *Rana* larvae (Anura: Ranidae). J. Morphol. 264, 34–52.
Leysen, H., Jouk, P., Brunain, M., Christiaens, J., Adriaens, D., 2010. Cranial architecture of tube-snouted gasterosteiformes (*Syngnathus rostellatus* and *Hippocampus capensis*). J. Morphol. 271, 255–270.
Lauder, G.V., 1985. Aquatic feeding in lower vertebrates. In: Hildebrand, M., Bramble, D.M., Liem, K.F., Wake, D.B. (Eds.), Functional Vertebrate Morphology. The Belknap Press (Harvard University Press, Cambridge, pp. 210–229.
Liem, K.F., 1978. Modulatory multiplicity in the functional repertoire of the feeding mechanism in cichlid fishes. I. Piscivores. J. Morphol. 158, 323–360.
Meyers, J.J., Herrel, A., Birch, J., 2002. Scaling of morphology, bite force and feeding kinematics in an iguanian and a scleroglossan lizard. In: Aerts, P., D'Aout, K., Herrel, A., Van Damme, R. (Eds.), Topics in Functional and Ecological Vertebrate Morphology. Shaker, Maastricht, Netherlands, pp. 47–62.
Muller, M., Osse, J.W.M., Verhagen, J.H.G., 1982. A quantitative hydrodynamical model of suction feeding in fish. J. Theor. Biol. 95, 49–79.
Muller, M., 1987. Optimization principles applied to the mechanism of neurocranium levation and mouth bottom depression in bony fishes (Halecostomi). J. Theor. Biol. 126, 343–368.
Markey, M.J., Main, R.P., Marshall, C.R., 2006. *In vivo* cranial suture function and suture morphology in the extant fish *Polypterus*: implications for inferring skull function in living and fossil fish. J. Exp. Biol. 209, 2085–2102.
Reilly, S.M., 1995. The ontogeny of aquatic feeding behaviour in *Salamandra salamandra*: stereotypy and isometry in feeding kinematics. J. Exp. Biol. 198, 701–708.
Richard, B.A., Wainwright, P.C., 1995. Scaling of the feeding mechanism of largemouth bass (*Micropterus salmoides*): kinematics of prey capture. J. Exp. Biol. 198, 419–433.
Robinson, M.P., Motta, P.J., 2002. Patterns of growth and the effects of scale on the feeding kinematics of the nurse shark (*Ginglymostoma cirratum*). J. Zool. (London) 256, 449–462.
Roos, G., Van Wassenbergh, S., Herrel, A., Adriaens, D., Aerts, P., 2010. Snout allometry in seahorses: insights on optimisation of pivot feeding performance during ontogeny. J. Exp. Biol. 213, 2184–2193.
Roos, G., Van Wassenbergh, S., Herrel, A., Aerts, P., 2009. Kinematics of suction feeding in the seahorse *Hippocampus reidi*. J. Exp. Biol. 212, 3490–3498.
Schmidt-Nielsen, K., 1984. Scaling: Why is Animal Size so Important?. Cambridge University Press, Cambridge.
Svanbäck, R., Wainwright, P.C., Ferry-Graham, L.A., 2002. Linking cranial kinematics, buccal pressure, and suction feeding performance in largemouth bass. Physiol. Biochem. Zool. 75, 532–543.
Vincent, S., Herrel, A., Irschick, D.J., 2004. Ontogeny of intersexual head shape and prey selection in the pitviper *Agkistrodon piscivorus*. Biol. J. Linn. Soc. 81, 151–159.
Van Wassenbergh, S., Aerts, P., Herrel, A., 2006. Hydrodynamic modelling of aquatic suction performance and intra-oral pressures: limitations for comparative studies. J. R. Soc. Interface 3, 507–514.
Van Wassenbergh, S., Roos, G., Genbrugge, A., Leysen, H., Aerts, P., Adriaens, D., Herrel, A., 2009a. Suction is kid's play: extremely fast suction in newborn seahorses. Biol. Lett. 5, 200–203.
Van Wassenbergh, S., Aerts, P., 2009. Aquatic suction feeding dynamics: insights from computational modelling. J. R. Soc. Interface 6, 149–158.
Van Wassenbergh, S., Strother, J.A., Flammang, B.E., Ferry-Graham, L.A., Aerts, P., 2008. Extremely fast prey capture in pipefish is powered by elastic recoil. J. R. Soc. Interface 5, 285–296.
Van Leeuwen, J.L., Muller, M., 1984. Optimum sucking techniques for predatory fish. Trans. Zool. Soc. London 37, 137–169.
Van Wassenbergh, S., Lieben, T., Herrel, A., Huysentruyt, F., Geerinckx, T., Adriaens, D., Aerts, P., 2009b. Kinematics of benthic suction feeding in Callichthyidae and Mochokidae, with functional implications for the evolution of food scraping in catfishes. J. Exp. Biol. 212, 116–125.
Wainwright, P.C., Day, S.W., 2007. The forces exerted by aquatic suction feeders on their prey. J. R. Soc. Interface 4, 533–560.
Wainwright, P.C., Lauder, G.V., 1986. Feeding biology of sunfishes: patterns of variation in prey capture. Zool. J. Linn. Soc. London 88, 217–228.